https://doi.org/10.1016/j.energy.2021.120345 **This is the Pre-Published Version.**

Two-stage Robust Distribution System Operation by Coordinating Electric Vehicle Aggregator Charging and Load Curtailments

Xi Lu [a], Shiwei Xia [b,*], Wei Gu [a], Ka Wing Chan [c] and Mohammad Shahidehpour [d]

* Corresponding author (e-mail: s.w.xia@ncepu.edu.cn)

[a] School of Electrical Engineering, Southeast University, Nanjing 210096, China.

[b] School of Electrical and Electronic Engineering, North China Electric Power University, Beijing 102206, China.

[c] Department of Electrical Engineering, The Hong Kong Polytechnic University, Hung Hom, Hong Kong SAR, China.

[d] Illinois Institute of Technology, Chicago, IL 60616 USA.

Email addresses: harry.lu@connect.polyu.hk (X. Lu), s.w.xia@ncepu.edu.cn (S. Xia), wgu@seu.edu.cn (W. Gu), eekwchan@polyu.edu.hk (K. W. Chan), ms@iit.edu (M. Shahidehpour).

Abstract

In this paper, a comprehensive two-stage robust distribution system operation model is proposed by adjusting the charging of electric vehicle aggregators (EVAs) and curtailing loads. Because uncertainties in EVA charging demands are involved in the second stage of the adopted two-stage framework, distributionally robust optimization is used to improve the average economic performance of the proposed model, and security of distribution system operation is guaranteed by applying the Farkas lemma and robust optimization. The proposed model is solved by iteratively adding optimality cuts and feasibility cuts through a novel constraint generation algorithm, whose mathematical proof is provided. The case studies show that the proposed model is capable of properly handling EVA uncertainties and coordinating EVA charging and load curtailments. The optimal coordination depends on several key parameters including the cost coefficients of delaying EVA charging and curtailing loads, the limits on delaying EVA charging, the system load level, and the EVA uncertainty level.

Keywords

Distribution system, Electric vehicle aggregator, Load curtailment, Economic performance, System security, Distributionally robust optimization, Robust Optimization

Highlights:

- A two-stage robust distribution system operation model is proposed.
- Electric vehicle aggregator charging and load curtailments are coordinated.
- Average economic performance is improved by distributionally robust optimization.
- System security is guaranteed through robust optimization and Farkas lemma.
- The proposed model is solved through a novel constraint generation algorithm.

Nomenclature

A. Abbreviations and acronyms

CCG	Column-and-constraint Generation
EV	Electric vehicle
EVA	Electric vehicle aggregator

DSO Distribution system operator

SO Stochastic optimization

DRO Distributionally robust optimization

AVR Automatic voltage regulator

B. Coefficients and variables

$c_{\text{res}}^{t,i}$ Cost coefficient of load curtailment reserves at Node i in Hour t

$c_{\text{cur}}^{t,i}$ Compensation coefficient for load curtailments at Node i in Hour t

$c_{\text{EVA}}^{t,i}$ Compensation coefficient for delayed EVA charging at Node i in Hour t

α_{EVA}^{i} EVA power factor at Node i

$p_{\text{load}}^{t,i}$ Active load at Node i in Hour t

$q_{\text{load}}^{t,i}$ Reactive load at Node i in Hour t

v_0 Base voltage

S_{EVA} Set of nodes with EVA

S_{AVR} Set of nodes with AVR

S_{dis} Set of all nodes in the distribution system

$S_{\text{p}}(i)$ Parent node of Node i

$S_{\text{c}}(i)$ Set of child nodes of Node i

$r_{i,j}$ Line resistance between Node i and j

$x_{i,j}$ Line reactance between Node i and j

$l_{\text{cur}}^{t,i}$ Limit on maximum load curtailment reserves at Node i in Hour t

$l_{\text{delay}}^{t,i}$ Limit on maximum delayed EVA charging at Node i in Hour t

l_{AVR}^{i} Limit on maximum AVR output at Node i

Δt An hour

$r_{\text{cur}}^{t,i}$ Load curtailment reserves at Node i in Hour t

$\boldsymbol{x}$ Vector of first-stage variables

$p_{\text{cur}}^{t,i}$ Curtailed active loads at Node i in Hour t

$q_{\text{AVR}}^{t,i}$ AVR output at Node i in Hour t

$e_{\text{delay}}^{t,i}$ Delayed EVA charging at Node i in Hour t

$p_{\text{EVA}}^{t,i}$ EVA charging power at Node i in Hour t

$f_{\text{p}}^{t,i,j}$ Active power flow from Node i to j in Hour t

$f_{\text{q}}^{t,i,j}$ Reactive power flow from Node i to j in Hour t

$v_{t,i}$ Voltage at Node i in Hour t

$\boldsymbol{y}$ Vector of second-stage variables

$\xi_{\text{EVA}}^{t,i}$ Uncertain active EVA charging demand at Node i in Hour t

$\mu_{t,i}$ Statistical expectation of $\xi_{\text{EVA}}^{t,i}$

$\boldsymbol{\xi}$ Vector of $\xi_{\text{EVA}}^{t,i}$ for all t and $i \in S_{\text{EVA}}$

$\boldsymbol{\mu}$ Vector of $\mu_{t,i}$ for all t and $i \in S_{\mathrm{EVA}}$

$\boldsymbol{\Sigma}$ Statistical covariance matrix of $\boldsymbol{\xi}$

f_{ξ} Distribution of $\boldsymbol{\xi}$

S_{ξ} Ellipsoidal support of $\boldsymbol{\xi}$

$A(\xi)$ Ambiguity set of $\boldsymbol{\xi}$

I. Introduction

As environmental issues become of more concern to the public, and electric vehicle (EV) technology continues to develop, the number of EVs is growing rapidly. J.P. Morgan estimated that EVs and hybrid vehicles would account for 30% of all vehicle sales by 2025 and 60% by 2030 [1], while India plans to forbid the sales of traditional vehicles by 2030 [2].

The penetration of EVs results in considerable charging demands, which are influenced by uncertain EV traveling behavior [3],[4]. Negative impacts on the distribution system can be incurred without appropriate control measures [5],[6]. Therefore, much work has been done on scheduling EV charging. In [7], EVs are utilized as distributed generators to improve the characteristics of the distribution system operation, including voltage profile and energy production costs. [8] seeks an optimal EV charging strategy that minimizes the power supply costs and unmet charging demand. Imbalances in the system are alleviated by scheduling EV charging in [9]. [10] optimized the EV charging strategy by considering the traffic system. However, when EVs become even more popular in the future, it will be quite difficult for power system operators to directly coordinate a large number of EVs [11]. Instead, it is more viable to let electric vehicle aggregators (EVAs) each regulate a limited number of EVs [12],[13] so that system operators only need to dispatch several EVAs rather than numerous EVs. For example, EVAs are controlled to match uncertain wind power in [11], and [14] proposed a hierarchical framework to dispatch EVAs. However, [11] and [14] neglected network constraints. [15] coordinated generators and EVAs to minimize the total operation costs considering the network constraints, but ignores the EVA uncertainties. [16] established a distribution system operation model by dispatching EVAs and considering EVA uncertainties. However, it has the following problems: First, the probabilistic distribution of uncertain EVA charging demand is assumed to be known accurately, which is unrealistic because information about uncertainties is usually limited. In addition, although the model in [16] properly guarantees system security, it uses piecewise linearization approximations to calculate the average operation costs, which is inaccurate. [17] appropriately models the uncertainty in EVA charging demands and evaluates the costs affected by uncertainties, but no other flexible resources apart from EVAs are considered. In fact, load curtailments often play an important role in distribution system operation [18].

In consideration of the research gaps in the literature, a model is proposed in this paper to coordinate the EVA charging strategy and load curtailments in distribution system operation. The basic assumptions of this model are as follows: (1) from the perspective of the distribution system operator (DSO), EVAs are loads that are always connected to the system; (2) because of uncertainties related to individual EVs, there are uncertainties in the overall EVA charging demands, which are the random variables considered in the proposed model and are represented by $\boldsymbol{\xi}$ according to Nomenclature; (3) as EVAs can adjust the charging of EVs before they depart, EVAs are able to provide flexibility for distribution system operation, which means that EVA charging demands can be delayed by DSO to some extent; (4) the model is proposed for DSO to dispatch EVAs and does not study how EVAs control EVs, as this is not the concern of DSO.

In terms of dealing with uncertainties, some studies such as [19] and [20] established single-stage models by assuming that recourse actions are affine functions of uncertainties. Such an assumption greatly limits the possible recourse actions and thus can be very conservative. Another option for problems involving uncertainties is adopting a two-stage framework, whose first and second stage model the operation before and after the realization of uncertainties, respectively. Unlike single-stage models, two-stage models have no additional limitation on recourse actions, which can be determined optimally by solving the second-stage problem. As a result, these models have found several applications. In [21], a two-stage model was established for hybrid microgrids in rural areas. [22] managed urban multi-energy systems using a two-stage framework. A two-stage operation model of grid-connected microgrids was proposed in [23]. To accurately model the recourse actions with respect to uncertainties, a two-stage framework is adopted in this paper. As the second-stage problem depends on first-stage decisions in two-stage

frameworks, improper first-stage decisions could lead to inferior results in the second stage. Therefore, the second-stage problem is considered in the first-stage problem of the proposed model to ensure that proper first-stage decisions are made.

In terms of evaluating uncertainty-affected costs, some studies adopted stochastic optimization (SO), which represents uncertainties by a set of scenarios in optimization problems [24],[25]. However, a large number of scenarios are needed to guarantee the performance of SO, which leads to a heavy computational burden [26]. It is also difficult to generate proper scenarios when little information about uncertainties is available. Because of the limitations of SO, an advanced approach called distributionally robust optimization (DRO) is adopted to evaluate the average uncertainty-affected costs and improve the average economic performance of the proposed model. Considering the limited information about uncertainties, the proposed model uses DRO to establish an ambiguity set that contains a family of possible distributions for uncertainties according to certain available information, such as statistical uncertainty moments [27],[28]. The worst distribution in the ambiguity set is focused on to hedge against ambiguity in the uncertainty distribution [29],[30]. Unlike models using SO, the proposed model does not require an excessive number of scenarios and thus avoids a heavy computational burden.

Although DRO is good at evaluating average uncertainty-affected costs because of its worst-distribution orientation, it cannot properly guarantee system security with respect to the worst possible uncertainty realization. In contrast to DRO, robust optimization focuses on the worst possible uncertainty realization [31],[32] and is used to ensure secure system operation with the aid of Farkas lemma under the adopted two-stage framework. By taking advantage of both RO and DRO, the proposed model properly handles EVA uncertainties in terms of both economic performance and system security.

The column-and-constraint generation (CCG) algorithm is often used to solve two-stage models. For example, CCG algorithm is used to solve two-stage energy hub operation in the environment of energy markets in [33], decentralized optimization of multi-energy systems with electricity and heat using two-stage formulations in [34], and a two-stage operation model of integrated energy systems with gas in [35]. However, because the proposed model uses DRO to evaluate uncertainty-affected costs, CCG algorithm is not applicable. In the formulation of the proposed model, a tailor-made constraint generation algorithm is used in the solution. Further discussions about the traditional CCG algorithm and the tailor-made constraint generation algorithm are made in Section IV.

The contributions of this paper are summarized below.

(1) A two-stage robust model is proposed to coordinate EVA charging and load curtailments for distribution system operation considering the uncertainties in EVA charging demands.

(2) Under the adopted two-stage framework, distributionally robust optimization is used to improve the average economic performance of the proposed model, and robust optimization is adopted to guarantee system security with the aid of the Farkas lemma.

(3) The proposed model is solved using a novel constraint generation algorithm, and its effectiveness is illustrated through comprehensive case studies.

The remainder of this paper is organized as follows. Section II presents the formulation of the proposed model. In Section III, the proposed model is transformed into deterministic forms. Based on the transformation in Section III, the solution algorithm is presented in Section IV. Case studies are presented in Section V to demonstrate the model proposed in Section II. Finally, the conclusions are presented in Section VI.

II. Problem Formulation

The first and second stages of the proposed model are before and after the realization of uncertainties in EVA charging demands, respectively. In the first stage, DSO purchases reserves for load curtailments at each node of the distribution system. In the second stage, DSO delays EVA charging, curtails loads, and determines the output of automatic voltage regulators (AVRs) according to uncertainty realizations. The loads curtailed in the second stage cannot exceed the reserves that DSO purchased in the first stage. With such an arrangement, energy users in the distribution system could know in advance the largest loads that may be curtailed and make corresponding preparations.

Delaying EVA charging and curtailing loads can both ensure secure distribution system operation in peak hours with high loads, but they achieve it in different ways. With load curtailments, the problems caused by excessive loads can be solved, and the

corresponding costs are known immediately. No correlation between different hours is incurred by load curtailments. In contrast, delayed EVA charging demands do not vanish like curtailed loads but are shifted to later hours that have fewer loads, which means that operation in different hours will be correlated because of delayed EVA charging demands. In addition, depending on the specific circumstances, EVA charging demands may be delayed for one hour or several hours. Therefore, the cost of delaying EVA charging is more complicated than that of curtailing loads. With their respective features, either delaying EVA charging or curtailing loads is more advantageous in different situations. Therefore, the proposed model coordinates the use of both approaches to achieve the optimal distribution system operation.

Because the load curtailment reserves are decided in the first stage and fixed in the second stage, the second-stage problem depends on the first-stage decisions. To ensure the overall optimal results in the two stages, the first-stage problem should also consider second-stage costs, which are influenced by uncertainty realizations. It should be noted that there is no universally optimal method for evaluating uncertainty-affected costs. The most appropriate method depends on the attitude of decision makers toward risks. In some studies, including [21]-[23], the second-stage cost under the worst uncertainty realization is considered in the objective. Such an approach is suitable for decision makers who cannot take any risk but is overly conservative because the worst uncertainty realization rarely occurs. Therefore, a more reasonable way for most decision makers is to minimize the sum of first-stage costs and average second-stage costs over all possible uncertainty realizations in the first-stage problem. However, as discussed in Section I, there is ambiguity in the uncertainty distribution, and thus the average second-stage costs cannot be obtained exactly. Some studies, such as [25] and [36], directly neglect such ambiguity and consider the average costs under the assumed uncertainty distribution. If the actual uncertainty distribution is very close to the assumed distribution, their models can exhibit good performance. If not, the performance of their models will be significantly degraded [37]. Therefore, to be cautious under the ambiguity in the uncertainty distribution, the first-stage problem of the proposed model uses DRO to calculate the worst possible expectation of second-stage costs with respect to all distributions in the ambiguity set $A(\boldsymbol{\xi})$, which is also adopted and validated in the literature, such as in [38] and [39].

A. The First-stage Problem

The first-stage problem is described by (1)-(2). The objective (1) considers the costs that DSO needs to pay in both stages. The first item in (1) is the first-stage cost, that is, the cost of reserves for load curtailments at all nodes in all hours, and is a linear function of load curtailment reserves $r_{\text{cur}}^{t,i}$. $\Psi(\boldsymbol{x},\boldsymbol{\xi})$ in (1) is the optimal second-stage cost and needs to be obtained by solving the second-stage problem. $\boldsymbol{x}$ is the vector of all first-stage decision variables, that is, $r_{\text{cur}}^{t,i}$ for all t and $i \in S_{\text{dis}}$. E[] is the operator that calculates expectations. Therefore, the second part of (1) is the worst expected second-stage cost with respect to all possible distributions f_{ξ} in the ambiguity set $A(\boldsymbol{\xi})$. (2) constrains the reserves for load curtailments at all nodes in all hours to be non-negative and smaller than their limits.

$$\min \sum_{t=1,\dots,24} \sum_{i \in S_{\text{dis}}} c_{\text{res}}^{t,i} r_{\text{cur}}^{t,i} + \max_{f_{\xi} \in A(\xi)} \mathrm{E}\left[\Psi\left(\boldsymbol{x},\boldsymbol{\xi}\right)\right] \tag{1}$$

$$s.t. \quad 0 \le r_{\text{cur}}^{t,i} \le l_{\text{cur}}^{t,i}, \forall i \in S_{\text{dis}}, \forall t \tag{2}$$

B. The Second-stage Problem

The second-stage problem is given in (3)-(12). $c_{\text{EVA}}^{t,i} e_{\text{delay}}^{t,i}$ and $c_{\text{cur}}^{t,j} p_{\text{cur}}^{t,j}$ in (3) are compensations for delayed EVA charging and curtailed loads, respectively. (4) requires the EVA charging power $p_{\text{EVA}}^{t,i}$ to be non-negative. Delayed EVA charging $e_{\text{delay}}^{t,i}$ is the EVA charging demand that has not been met, that is, the difference between EVA charging demands and the energy supplied, as shown in (5). It is constrained to be non-negative and smaller than the limits in (6). (7) requires the curtailed loads $p_{\text{cur}}^{t,i}$ to be non-negative and smaller than the reserves $r_{\text{cur}}^{t,i}$ scheduled in the first stage. AVR outputs $q_{\text{AVR}}^{t,i}$ are restricted to be non-negative and lower than the AVR capacity l_{AVR}^{i} in (8). According to the linearized power flow model for distribution systems in [40], (9) and (10) give active and reactive power flows, respectively, and the node voltage is given in (11). As shown in (9) and (10), the power flow on a feeder is the sum of the power flows on all its child feeders and the net load at the node connecting it to its child feeders. In (10), $q_{\text{load}}^{t,i} \cdot p_{\text{cur}}^{t,i} / p_{\text{load}}^{t,i}$ is the curtailed reactive load, and $p_{\text{EVA}}^{t,i} \sqrt{1 - \left(\alpha_{\text{EVA}}^{i}\right)^2} / \alpha_{\text{EVA}}^{i}$ is the reactive EVA charging power. According to

(11), the difference between the voltages of two adjacent nodes is simply the voltage drop on the feeder connecting them. (12) constrains the node voltage within the safe range. It should be noted that $\xi_{\mathrm{EVA}}^{t,i}$ in (5) is the uncertainty involved in the proposed model.

$$\min \sum_{t=1,\ldots,24}\left(\sum_{i\in S_{\mathrm{EVA}}} c_{\mathrm{EVA}}^{t,i} e_{\mathrm{delay}}^{t,i} + \sum_{j\in S_{\mathrm{dis}}} c_{\mathrm{cur}}^{t,j} p_{\mathrm{cur}}^{t,j}\Delta t\right) \tag{3}$$

$$s.t.\ \ p_{\mathrm{EVA}}^{t,i} \geq 0, \forall i \in S_{\mathrm{EVA}}, \forall t \tag{4}$$

$$e_{\mathrm{delay}}^{t,i} = \sum_{\hat{t}=1,\ldots,t}\left(\xi_{\mathrm{EVA}}^{\hat{t},i} - p_{\mathrm{EVA}}^{\hat{t},i}\right)\cdot\Delta t, \forall i \in S_{\mathrm{EVA}}, \forall t \tag{5}$$

$$0 \leq e_{\mathrm{delay}}^{t,i} \leq l_{\mathrm{delay}}^{t,i}, \forall i \in S_{\mathrm{EVA}}, \forall t \tag{6}$$

$$0 \leq p_{\mathrm{cur}}^{t,i} \leq r_{\mathrm{cur}}^{t,i}, \forall i \in S_{\mathrm{dis}}, \forall t \tag{7}$$

$$0 \leq q_{\mathrm{AVR}}^{t,i} \leq l_{\mathrm{AVR}}^{i}, \forall i \in S_{\mathrm{AVR}}, \forall t \tag{8}$$

$$f_{\mathrm{p}}^{t,S_{\mathrm{p}}(i),i} = p_{\mathrm{load}}^{t,i} - p_{\mathrm{cur}}^{t,j} + p_{\mathrm{EVA}}^{t,i} + \sum_{j\in S_{\mathrm{c}}(i)} f_{\mathrm{p}}^{t,i,j},\ \forall i \in S_{\mathrm{dis}}/\{1\}, \forall t \tag{9}$$

$$f_{q}^{t,S_{\mathrm{p}}(i),i} = q_{\mathrm{load}}^{t,i} - q_{\mathrm{load}}^{t,i}\cdot p_{\mathrm{cur}}^{t,i} / p_{\mathrm{load}}^{t,i} + \sum_{j\in S_{\mathrm{c}}(i)} f_{q}^{t,i,j} - q_{\mathrm{AVR}}^{t,i} + p_{\mathrm{EVA}}^{t,i}\sqrt{1-\left(\alpha_{\mathrm{EVA}}^{i}\right)^2} / \alpha_{\mathrm{EVA}}^{i}, \forall i \in S_{\mathrm{dis}}/\{1\}, \forall t \tag{10}$$

$$v_{t,i} + \left(r_{S_{\mathrm{p}}(i),i}\cdot f_{\mathrm{p}}^{t,S_{\mathrm{p}}(i),i} + x_{S_{\mathrm{p}}(i),i}\cdot f_{\mathrm{q}}^{t,S_{\mathrm{p}}(i),i}\right)/v_0 = v_{t,S_{\mathrm{p}}(i)}, \forall i \in S_{\mathrm{dis}}/\{1\}, \forall t \tag{11}$$

$$0.95v_0 \leq v_{t,i} \leq 1.05v_0, \forall i \in S_{\mathrm{dis}}, \forall t \tag{12}$$

Each equality constraint in (3)-(12) can be replaced by a set of two inequality constraints. For example, $e_{\mathrm{delay}}^{t,i} = \sum_{\hat{t}=1,\ldots,t}\left(\xi_{\mathrm{EVA}}^{\hat{t},i} - p_{\mathrm{EVA}}^{\hat{t},i}\right)\cdot\Delta t$ in (5) is equivalent to the combination of $e_{\mathrm{delay}}^{t,i} \leq \sum_{\hat{t}=1,\ldots,t}\left(\xi_{\mathrm{EVA}}^{\hat{t},i} - p_{\mathrm{EVA}}^{\hat{t},i}\right)\cdot\Delta t$ and $e_{\mathrm{delay}}^{t,i} \geq \sum_{\hat{t}=1,\ldots,t}\left(\xi_{\mathrm{EVA}}^{\hat{t},i} - p_{\mathrm{EVA}}^{\hat{t},i}\right)\cdot\Delta t$. Therefore, the compact form of the second-stage problem can be written as (13)-(15), where $\boldsymbol{y}$ is the vector of the second-stage decision variables and is made up of $e_{\mathrm{delay}}^{t,i}$, $p_{\mathrm{cur}}^{t,j}$ and $q_{\mathrm{AVR}}^{t,k}$ for all t, $i \in S_{\mathrm{EVA}}$, $j \in S_{\mathrm{dis}}$, and $k \in S_{\mathrm{AVR}}$. Other variables in (3)-(12), including $p_{\mathrm{EVA}}^{t,i}$, $f_p^{t,i,j}$, $f_q^{t,i,j}$, and $v_{t,i}$ can be represented by affine functions of $\boldsymbol{y}$.

$$\min_{\boldsymbol{y}}\ \boldsymbol{a}'\cdot\boldsymbol{y} \tag{13}$$

$$s.t.\ \ \boldsymbol{B}\cdot\boldsymbol{y} \leq \boldsymbol{b} - \boldsymbol{C}\cdot\boldsymbol{x} - \boldsymbol{D}\cdot\boldsymbol{\xi} \tag{14}$$

$$\boldsymbol{y} \geq \boldsymbol{0} \tag{15}$$

III. Problem Transformation

If there is no uncertainty in EVA charging demands, the two stages of the proposed model can be merged, and it will become a deterministic linear optimization problem, which can be directly solved. The contents described in Sections III and IV are then not required. However, with uncertainties, the second-stage problem of the proposed model becomes deterministic after uncertainties are realized in the second stage, while the first-stage problem is before uncertainty realizations and is not deterministic because of the second part of (1).

To rewrite (1) into explicit and deterministic forms, DRO is first used to transform the second part of (1). (16) is the adopted ambiguity set, which means that all possible distributions satisfying (16) are taken into consideration by DRO. The first row in (16) constrains all possible realizations of $\boldsymbol{\xi}$ within the ellipsoidal support set $S_{\boldsymbol{\xi}}$. The second and third rows in (16) depict the uncertainty expectation and covariance matrix, respectively. The third row in (16) is equivalent to $\boldsymbol{\Sigma} - \mathrm{E}[(\boldsymbol{\xi}-\boldsymbol{\mu})(\boldsymbol{\xi}-\boldsymbol{\mu})'] \succcurlyeq \mathbf{0}$, which requires $\boldsymbol{\Sigma} - \mathrm{E}[(\boldsymbol{\xi}-\boldsymbol{\mu})(\boldsymbol{\xi}-\boldsymbol{\mu})']$ to be a positive semidefinite matrix. Given (16), the second item in (1) can be rewritten explicitly as (17)-(21) by introducing the concept of integral in mathematics. (17) corresponds to the second part of (1). (18) requires the probability density function $f_{\boldsymbol{\xi}}(\boldsymbol{\xi})$ to be positive. (19)-(21) are rewritten versions of the three rows of (16). Because $\boldsymbol{\xi}$ is continuous, the problem (17)-(21) needs to be optimized over $f_{\boldsymbol{\xi}}(\boldsymbol{\xi})$ of infinite realizations of $\boldsymbol{\xi}$, which makes it impossible to handle the problem directly and requires further transformation. It should be noted that the proposed model is regarded as a mathematical problem from now on. The mathematical transformations in the following parts of Sections III and IV do not have corresponding physical interpretations, but all aim to solve the proposed model optimally and efficiently and thus facilitate DSO to make proper decisions.

$$A(\xi)=\left\{ f_{\xi} \left| \begin{array}{l} \boldsymbol{\xi} \in S_{\xi} \\ \mathrm{E}[\boldsymbol{\xi}]=\boldsymbol{\mu} \\ \mathrm{E}\left[(\boldsymbol{\xi}-\boldsymbol{\mu})(\boldsymbol{\xi}-\boldsymbol{\mu})'\right] \circ \ \boldsymbol{\Sigma} \end{array} \right. \right\} \tag{16}$$

$$\max_{f_{\xi}} \int \Psi(\boldsymbol{x},\boldsymbol{\xi}) f_{\xi}(\boldsymbol{\xi}) \cdot d\boldsymbol{\xi} \tag{17}$$

$$s.t. \ f_{\xi}(\boldsymbol{\xi}) \geq 0, \forall \boldsymbol{\xi} \in S_{\xi} \tag{18}$$

$$\int_{S_{\xi}} f_{\xi}(\boldsymbol{\xi}) \cdot d\boldsymbol{\xi} = 1 \tag{19}$$

$$\int_{S_{\xi}} \boldsymbol{\xi} \cdot f_{\xi}(\boldsymbol{\xi}) \cdot d\boldsymbol{\xi} = \boldsymbol{\mu} \tag{20}$$

$$\int_{S_{\xi}} (\boldsymbol{\xi}-\boldsymbol{\mu})(\boldsymbol{\xi}-\boldsymbol{\mu})' \ f_{\xi}(\boldsymbol{\xi}) \cdot d\boldsymbol{\xi} \circ \ \boldsymbol{\Sigma} \tag{21}$$

By using the duality theory [41],[42], the dual problem of (17)-(21) can be obtained as (22)-(24), where $\boldsymbol{H}$, $\boldsymbol{h}$, and h_0 are dual variables. $tr()$ in (22) calculates the trace of the matrix. To further transform (22)-(24), $\Psi(\boldsymbol{x},\boldsymbol{\xi})$ in (23) must be expressed in explicit forms. As the second-stage problem is a linear optimization problem, its optimal value, that is, $\Psi(\boldsymbol{x},\boldsymbol{\xi})$, is equal to that of its dual problem, whose compact form is given in (25)-(27) according to duality theory. $\boldsymbol{u}$ is the vector of the decision variables of the dual second-stage problem. Because (25)-(27) is also a linear optimization problem, its optimal value must be obtained at one of the extreme points of its feasible set U_1 if the second-stage problem (13)-(15) is feasible [43]. U_1 is not influenced by uncertainties, that is, $\xi_{\mathrm{EVA}}^{t,i}$, according to (28), so its extreme points are deterministic. Therefore, given that the second-stage problem (13)-(15) is feasible, $\Psi(\boldsymbol{x},\boldsymbol{\xi})$ can be obtained by enumerating the extreme points of U_1 as shown in (29), where $\boldsymbol{u}_{\mathrm{p}}^{i}$ is the i^{th} extreme point of U_1, and S_{p} is the set of all extreme points of U_1. Using (29), (23) can be rewritten as (30).

$$\min_{\boldsymbol{H},\boldsymbol{h},h_0} \ \mathrm{tr}(\boldsymbol{H}' \cdot \boldsymbol{\Sigma}) + \boldsymbol{h}' \cdot \boldsymbol{\mu} + h_0 \tag{22}$$

$$s.t. \ \boldsymbol{\xi}' \cdot \boldsymbol{H} \cdot \boldsymbol{\xi} + \boldsymbol{h}' \cdot \boldsymbol{\xi} + h_0 \geq \Psi(\boldsymbol{x},\boldsymbol{\xi}), \forall \boldsymbol{\xi} \in S_{\xi} \tag{23}$$

$$\boldsymbol{H} \pm \mathbf{0} \tag{24}$$

$$\max_{\boldsymbol{u}} \ (\boldsymbol{b} - \boldsymbol{C} \cdot \boldsymbol{x} - \boldsymbol{D} \cdot \boldsymbol{\xi})' \boldsymbol{u} \tag{25}$$

$$s.t. \ \boldsymbol{B}' \cdot \boldsymbol{u} \leq \boldsymbol{a} \tag{26}$$

$$\boldsymbol{u} \leq \mathbf{0} \tag{27}$$

$$U_1 = \left\{ \boldsymbol{u} \middle| \boldsymbol{B}' \cdot \boldsymbol{u} \le \boldsymbol{a}, \boldsymbol{u} \le \boldsymbol{0} \right\} \tag{28}$$

$$\Psi\left(\boldsymbol{x}, \boldsymbol{\xi}\right) = \max_{i \in S_{\mathrm{p}}} \left(\boldsymbol{b} - \boldsymbol{C} \cdot \boldsymbol{x} - \boldsymbol{D} \cdot \boldsymbol{\xi}\right)' \boldsymbol{u}_{\mathrm{p}}^{i} \tag{29}$$

$$\boldsymbol{\xi}' \cdot \boldsymbol{H} \cdot \boldsymbol{\xi} + \boldsymbol{h}' \cdot \boldsymbol{\xi} + h_0 \ge \left(\boldsymbol{b} - \boldsymbol{C} \cdot \boldsymbol{x} - \boldsymbol{D} \cdot \boldsymbol{\xi}\right)' \boldsymbol{u}_{\mathrm{p}}^{i}, \forall \boldsymbol{\xi} \in S_{\xi}, \forall i \in S_{\mathrm{p}} \tag{30}$$

According to Farkas lemma [44], the second-stage problem (13)-(15) is feasible if and only if (31) is infeasible. Obviously, the infeasibility of (31) is equivalent to (32). Because U_2 is a polyhedral cone, every element in it can be represented by a nonnegative linear combination of its extreme rays [45]. Therefore, (32) can be replaced by (33), where $\boldsymbol{u}_{\mathrm{r}}^{i}$ is the i^{th} extreme ray of U_2, and S_{r} is the set of all extreme rays of U_2 [46],[47].

$$\left\{ \begin{array}{c} \boldsymbol{u} \in U_2 \\ U_2 = \left\{ \boldsymbol{u} \middle| \boldsymbol{B}' \cdot \boldsymbol{u} \le \boldsymbol{0}, \boldsymbol{u} \le \boldsymbol{0} \right\} \\ \left(\boldsymbol{b} - \boldsymbol{C} \cdot \boldsymbol{x} - \boldsymbol{D} \cdot \boldsymbol{\xi}\right)' \boldsymbol{u} > 0 \end{array} \right\} \tag{31}$$

$$\left(\boldsymbol{b} - \boldsymbol{C} \cdot \boldsymbol{x} - \boldsymbol{D} \cdot \boldsymbol{\xi}\right)' \boldsymbol{u} \le 0, \forall \boldsymbol{\xi} \in S_{\xi}, \forall \boldsymbol{u} \in U_2 \tag{32}$$

$$\left(\boldsymbol{b} - \boldsymbol{C} \cdot \boldsymbol{x} - \boldsymbol{D} \cdot \boldsymbol{\xi}\right)' \boldsymbol{u}_{\mathrm{r}}^{i} \le 0, \forall \boldsymbol{\xi} \in S_{\xi}, \forall i \in S_{\mathrm{r}} \tag{33}$$

Now, the first-stage problem (1)-(2) can be rewritten as (34)-(38). (34) is obtained by replacing the second part of (1) with (22). (35) is the first-stage constraint on load curtailment reserves and is the same as (2). (37) is the same as (33) and guarantees the feasibility of the second-stage problem (13)-(15). (36) and (38) are derived from the transformation of the second part of (1) and ensure the optimality of the proposed model. (36) is the same as (24), and (38) is the same as (30), which is derived from (23). Uncertainties are involved in (37) and (38). As $S_{\boldsymbol{\xi}}$ is an ellipsoid, (37) can be replaced by its deterministic counterpart according to robust optimization [48],[49], and (38) can be transformed into deterministic forms by using S-lemma [50]. After all the discussed transformations, the first-stage problem finally becomes a deterministic semidefinite optimization problem.

$$\min \sum_{t=1,\ldots,24} \sum_{i \in S_{\mathrm{dis}}} c_{\mathrm{res}}^{t,i} r_{\mathrm{cur}}^{t,i} + \mathrm{tr}\left(\boldsymbol{H}' \cdot \boldsymbol{\Sigma}\right) + \boldsymbol{h}' \cdot \boldsymbol{\mu} + h_0 \tag{34}$$

$$s.t. \quad 0 \le r_{\mathrm{cur}}^{t,i} \le l_{\mathrm{cur}}^{t,i}, \forall i \in S_{\mathrm{dis}}, \forall t \tag{35}$$

$$\boldsymbol{H} \pm \boldsymbol{0} \tag{36}$$

$$\left(\boldsymbol{b} - \boldsymbol{C} \cdot \boldsymbol{x} - \boldsymbol{D} \cdot \boldsymbol{\xi}\right)' \boldsymbol{u}_{\mathrm{r}}^{i} \le 0, \forall \boldsymbol{\xi} \in S_{\xi}, \forall i \in S_{\mathrm{r}} \tag{37}$$

$$\boldsymbol{\xi}' \cdot \boldsymbol{H} \cdot \boldsymbol{\xi} + \boldsymbol{h}' \cdot \boldsymbol{\xi} + h_0 \ge \left(\boldsymbol{b} - \boldsymbol{C} \cdot \boldsymbol{x} - \boldsymbol{D} \cdot \boldsymbol{\xi}\right)' \boldsymbol{u}_{\mathrm{p}}^{i}, \forall \boldsymbol{\xi} \in S_{\xi}, \forall i \in S_{\mathrm{p}} \tag{38}$$

IV. Solution Algorithm

To introduce the algorithm that solves the proposed model more clearly, it is first briefly compared with the CCG algorithm, which is usually applied to solve two-stage models that consider the second-stage problem under the worst uncertainty realization. In each iteration of CCG algorithm, the worst uncertainty realization with respect to the current first-stage decision is found. Then, a deterministic problem is formed by considering the potential second-stage problems under the newly found and all previously found uncertainty realizations in the first stage. By solving this problem, an updated first-stage decision can be obtained. This process continues until the optimal solution is reached. More details about CCG algorithm can be found in [33]-[35]. Because the proposed model considers the average second-stage objective under the worst uncertainty realization, no particular uncertainty realization needs to be found, and CCG algorithm is not applicable. In contrast to the CCG algorithm, the process of the algorithm

proposed in this section has no physical but only a mathematical interpretation. However, its convergence criterion guarantees that Eq. (37) and (38) in the transformed first-stage problem (34)-(38) hold, which has the following physical interpretation. With (37), the feasibility of the second-stage problem can be guaranteed with respect to all possible uncertainty realizations. With (38), the sum of the first-stage costs and the average second-stage costs under the worst uncertainty distribution can be minimized.

After the transformation in Section III, the first-stage and second-stage problems are semidefinite and linear optimization problems, respectively, and can be solved by off-the-shelf solvers. However, the large numbers of $\boldsymbol{u}_{\mathrm{r}}^{i}$ and $\boldsymbol{u}_{\mathrm{p}}^{i}$ involved in (37) and (38) result in a large computational burden and make it impossible to solve the first-stage problem directly. Among these $\boldsymbol{u}_{\mathrm{r}}^{i}$ and $\boldsymbol{u}_{\mathrm{p}}^{i}$, only a few correspond to the active constraints of the first-stage problem and thus are necessary. In other words, most $\boldsymbol{u}_{\mathrm{r}}^{i}$ and $\boldsymbol{u}_{\mathrm{p}}^{i}$ can be ignored, which does not affect the quality of the obtained solution. To avoid the computational burden caused by these unnecessary $\boldsymbol{u}_{\mathrm{r}}^{i}$ and $\boldsymbol{u}_{\mathrm{p}}^{i}$, the first-stage problem is solved by a novel constraint generation algorithm that iteratively finds all necessary $\boldsymbol{u}_{\mathrm{r}}^{i}$ and $\boldsymbol{u}_{\mathrm{p}}^{i}$ based on the transformation described in Section III.

Under the constraint generation algorithm, the problem (34)-(38) is relaxed by considering only parts of $\boldsymbol{u}_{\mathrm{r}}^{i}$ and $\boldsymbol{u}_{\mathrm{p}}^{i}$ in (37) and (38), respectively. The optimal $\boldsymbol{H}$, $\boldsymbol{h}$, h_0, and $\boldsymbol{x}$ obtained from the relaxed problem of (34)-(38) are represented by $\boldsymbol{H}^*$, $\boldsymbol{h}^*$, ${h_0}^*$, and $\boldsymbol{x}^*$, based on which (39)-(41) and (42)-(45) can be generated. Before the constraint generation algorithm is discussed further, two propositions are introduced. The proofs of the two propositions are given in the Appendix.

$$\min_{\boldsymbol{\xi},\boldsymbol{u}} \ \boldsymbol{\xi}' \cdot \boldsymbol{H}^* \cdot \boldsymbol{\xi} + \left(\boldsymbol{h}^*\right)' \cdot \boldsymbol{\xi} + {h_0}^* - \left(\boldsymbol{b} - \boldsymbol{C} \cdot \boldsymbol{x}^* - \boldsymbol{D} \cdot \boldsymbol{\xi}\right)' \boldsymbol{u} \tag{39}$$

$$s.t. \ \ \boldsymbol{\xi} \in S_{\xi} \tag{40}$$

$$\boldsymbol{u} \in U_1 \tag{41}$$

$$\max_{\boldsymbol{\xi},\boldsymbol{u}} \ \left(\boldsymbol{b} - \boldsymbol{C} \cdot \boldsymbol{x}^* - \boldsymbol{D} \cdot \boldsymbol{\xi}\right)' \boldsymbol{u} \tag{42}$$

$$s.t. \ \ \boldsymbol{\xi} \in S_{\xi} \tag{43}$$

$$\boldsymbol{u} \in U_2 \tag{44}$$

$$\left(\boldsymbol{b} - \boldsymbol{C} \cdot \boldsymbol{x}^* - \boldsymbol{D} \cdot \boldsymbol{\xi}\right)' \boldsymbol{u} \le 1 \tag{45}$$

Proposition 1:

Given that $\boldsymbol{H} = \boldsymbol{H}^*$, $\boldsymbol{h} = \boldsymbol{h}^*$, $h_0 = {h_0}^*$, and $\boldsymbol{x} = \boldsymbol{x}^*$, (37) holds if and only if (39)-(41) is bounded.

Proposition 2:

The optimal $\boldsymbol{u}$ solved from (42)-(45) is either at the origin point or on an extreme ray of U_2.

According to Proposition 1, if (39)-(41) is unbounded, (37) does not hold for $\boldsymbol{H} = \boldsymbol{H}^*$, $\boldsymbol{h} = \boldsymbol{h}^*$, $h_0 = {h_0}^*$, and $\boldsymbol{x} = \boldsymbol{x}^*$, which indicates that some necessary $\boldsymbol{u}_{\mathrm{r}}^{i}$ are not considered in the relaxed problem of (34)-(38). If the optimal value of (39)-(41) is negative, it is obvious that (38) does not hold for $\boldsymbol{H} = \boldsymbol{H}^*$, $\boldsymbol{h} = \boldsymbol{h}^*$, $h_0 = {h_0}^*$, and $\boldsymbol{x} = \boldsymbol{x}^*$, which shows that some necessary $\boldsymbol{u}_{\mathrm{p}}^{i}$ are not considered in the relaxed problem of (34)-(38). If (39)-(41) is bounded and its optimal value is non-negative, (37) holds according to Proposition 1, and obviously (38) holds as well, indicating that the optimal solution of the first-stage problem has been obtained.

According to Proposition 2, the optimal $\boldsymbol{u}$ obtained from (42)-(45) is either at the origin point or on an extreme ray of U_2. When (37) does not hold, (32) also does not hold, which means that the optimal value of (42)-(45) is positive. Therefore, the optimal $\boldsymbol{u}$ obtained from (42)-(45) must be on an extreme ray of U_2 as it cannot be at the origin point, and it is just a necessary $\boldsymbol{u}_{\mathrm{r}}^{i}$ that has been missed by the relaxed problem of (34)-(38). Therefore, the (37) corresponding to the necessary $\boldsymbol{u}_{\mathrm{r}}^{i}$ obtained by solving (42)-(45) should be added to the relaxed problem of (34)-(38) and is called a feasibility cut because (37) guarantees the feasibility of the second-stage problem (13)-(15), as discussed in Section III.

As (39)-(41) is a linear optimization problem over $\boldsymbol{u}$ when $\boldsymbol{\xi}$ is fixed, the optimal $\boldsymbol{u}$ obtained from (39)-(41) must be an extreme point of U_1 and is just a necessary $\boldsymbol{u}_{\mathrm{p}}^{i}$ that has been missed by the relaxed problem of (34)-(38) when the optimal value of (39)-(41) is bounded and negative. Therefore, the (38) corresponding to the necessary $\boldsymbol{u}_{\mathrm{p}}^{i}$ obtained by solving (39)-(41) should be

added to the relaxed problem of (34)-(38), and is called an optimality cut because (38) ensures the optimality of the proposed model, as discussed in Section III.

Based on the above discussions, the constraint generation algorithm to solve the first-stage problem is shown in Fig. 1. It should be noted that optimality cuts will certainly be added during the constraint generation algorithm, while feasibility cuts may or may not be added, depending on the parameter settings. To be more specific, adding feasibility cuts ensures that sufficient load curtailment reserves are scheduled in the first stage; thus, the second-stage problem is feasible. However, if the second-stage problem is always feasible regardless of the first-stage decisions, no feasibility cut will be added. The term $(\boldsymbol{D}\cdot\boldsymbol{\xi})'\cdot\boldsymbol{u}$ in (39)-(41) and (42)-(45) makes the two problems non-convex. However, when $\boldsymbol{\xi}$ or $\boldsymbol{u}$ is fixed, (39)-(41) and (42)-(45) both become convex. Therefore, a heuristic algorithm is used to solve them, as shown in Fig. 2 [51].

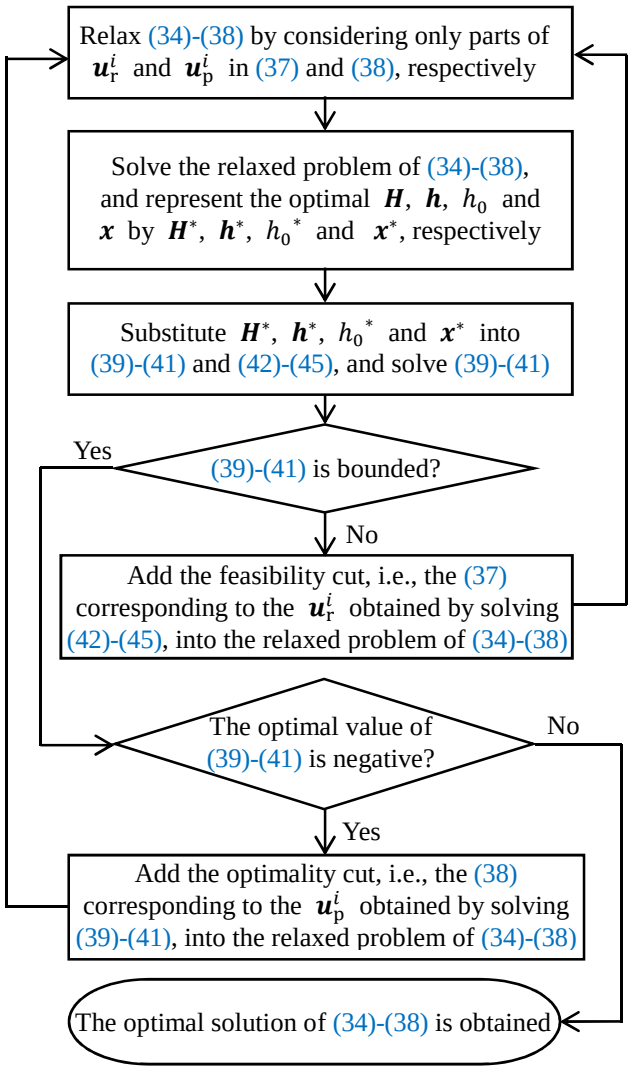

FIGURE 1. Constraint Generation algorithm to solve the first-stage problem

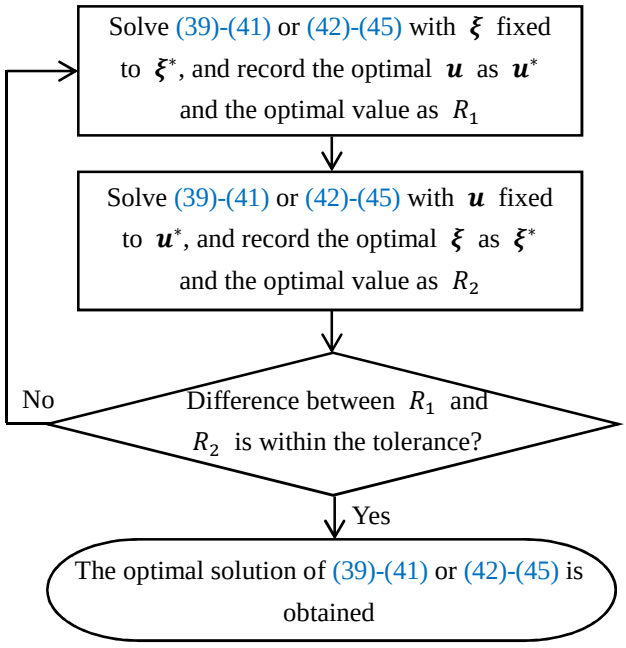

FIGURE 2. Heuristic algorithm to solve (39)-(41) and (42)-(45)

V. Case Studies

As discussed in Section II, the proposed model coordinates load curtailment and EVA charging to achieve secure and economical distribution system operation. Through a series of case studies, the coordination of load curtailment and EVA charging strategy, as well as the effects of uncertainties in EVA charging demands, are analyzed in this section. It should be noted that although the content in this section seems to have little correlation with Sections III and IV, all results presented are possible because of the mathematics outlined in Sections III and IV.

The 33-node distribution system from [52] is modified for the case studies conducted in this section. As shown in Fig. 3, Nodes 15, 18, and 33 each have an EVA, and Nodes 9, 11, 13, 16, 29, and 32 each have an AVR. The parameters of the distribution network are provided in the Appendix. The aggregated active loads in the distribution system are illustrated in Fig. 4. The considered EVAs are in residential areas. By assuming that EVs start charging at the rated power once they are connected to the distribution system, a series of EVA charging demands are simulated, and their statistical expectations, that is, $\mu_{t,i}$, are presented in Fig. 5, where the curves for EVAs at Nodes 15 and 18 are very close to each other. For space-saving purposes, the value of the covariance matrix of EVA charging demands, that is, $\mathbf{\Sigma}$, is not presented. The basic parameter settings are listed in Table I. In the following parts of Section V, the relevant parameters will take the values in Table I, unless otherwise stated. To test the proposed model, a series of random uncertainty realizations are generated according to normal distributions. The average performance of the proposed model is obtained by analyzing its results under different uncertainty realizations.

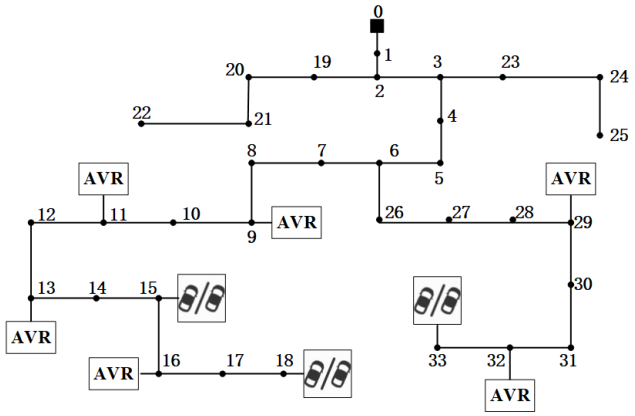

FIGURE 3. 33-node distribution network

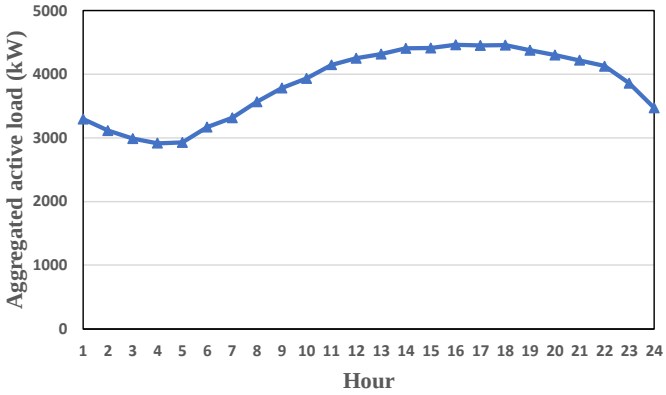

FIGURE 4. Aggregated active load in the distribution system

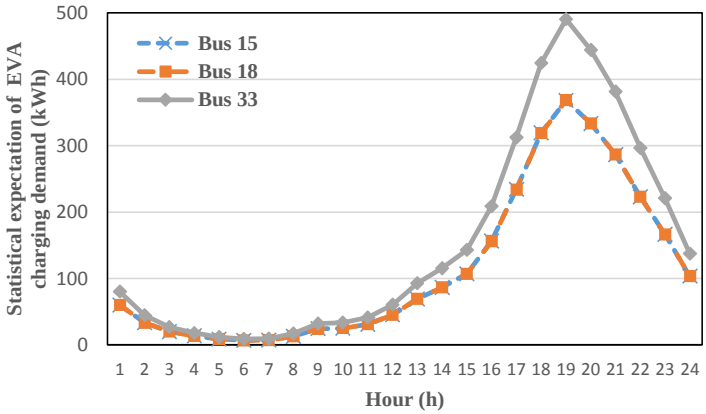

FIGURE 5. Statistical expectation of EVA charging demands, $\mu_{t,i}$

TABLE I BASIC PARAMETER SETTINGS

Cost coefficients of load curtailment reserves of all loads in all hours, $c_{\text{res}}^{t,i}$	0.5¢/kWh
Compensation coefficients for curtailment of all loads in all hours, $c_{\text{cur}}^{t,i}$	10¢/kWh
Compensation coefficients for delayed charging of all EVAs in all hours, $c_{\text{EVA}}^{t,i}$	6¢/kWh
Limits on outputs of all AVRs, l_{AVR}^{i}	500 kVar
Limits on delayed charging demands of all EVAs in all hours, $l_{\text{delay}}^{t,i}$ (times of the statistical expectation of EVA charging demands, $\mu_{t,i}$)	$2\mu_{t,i}$

A. Basic illustration of the proposed model

Four cases are considered in this part as listed in Table II. In Case A-I to A-III, EVA charging demand $\xi_{\text{EVA}}^{t,i}$ is assumed to be deterministic and equal to $0.75\mu_{t,i}$, $\mu_{t,i}$ and $1.25\mu_{t,i}$, respectively. As there is no uncertainty, the proposed model becomes a deterministic linear optimization problem and can be directly solved in Cases A-I to A-III. In Case A-IV, the proposed model is kept intact, which means that EVA charging demands are uncertain and thus their values are unknown in advance. Relevant results in Hour 18-22 under the four considered cases are shown in Fig. 6 to Fig. 9. Results in other hours are not included because this paper focuses on the coordination of EVA charging and load curtailment, and no load curtailment or delayed EVA charging is carried out during these hours. For a clearer illustration, only the results in hours when EVA charging is delayed or loads are curtailed are presented here and in the following parts of Section V. It should be noted that as the settings change, the hours with delayed EVA charging or load curtailment change as well. In Fig. 6 and 7, the results for Cases A-I to A-III are deterministic values, while the results for Case A-IV are average values with respect to uncertainties in EVA charging demands.

TABLE II CASES CONSIDERED IN SECTION V.A

Case	A-I	A-II	A-III	A-IV
Deterministic model?	Yes	Yes	Yes	No
Values of EVA charging demands $\xi_{\text{EVA}}^{t,i}$	$0.75\mu_{t,i}$	$\mu_{t,i}$	$1.25\mu_{t,i}$	Unknown in advance

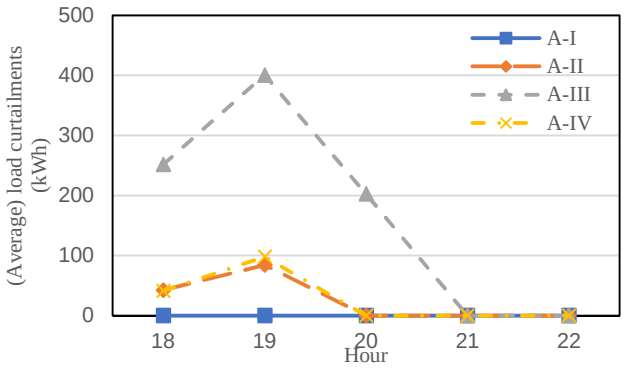

FIGURE 6. (Average) load curtailments under different settings in Section V.A

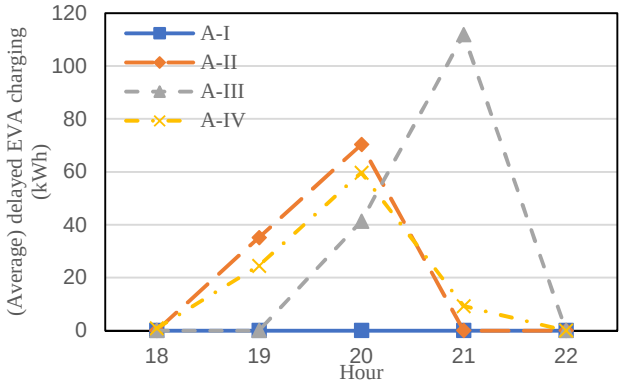

FIGURE 7. (Average) delayed EVA charging under different settings in Section V.A

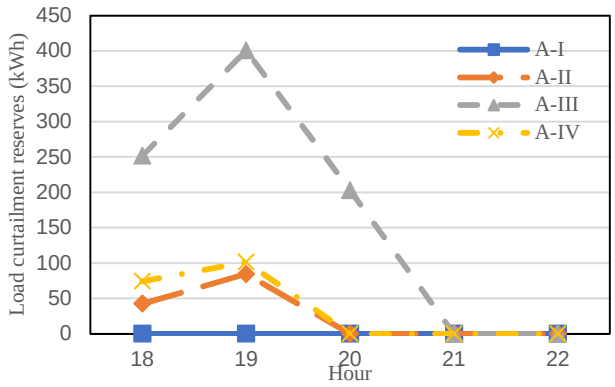

FIGURE 8. Load curtailment reserves under different settings in Section V.A

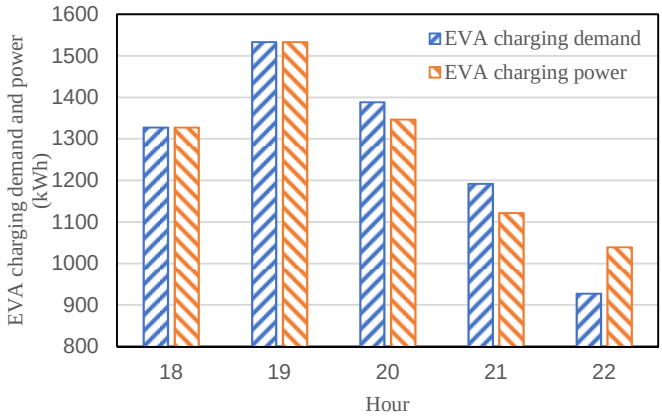

FIGURE 9. EVA charging demand and power in Case A-III

In Case A-I, EVA charging demands are relatively low, so there is no load curtailment or delayed EVA charging, as shown in Figs. 6 and 7. As EVA charging demands increase in Cases A-II and A-III, both load curtailment and delayed EVA charging are carried out to guarantee secure distribution system operation. In Cases A-I to A-III, the scheduled load curtailment reserves are the same as the curtailed loads because there is no uncertainty in the considered problem. However, when uncertainties in EVA charging demands are involved in Case A-IV, it becomes more complicated to decide how many reserves should be scheduled. If there are too many scheduled reserves, a part of the corresponding costs will be unnecessary under relatively low uncertainty realizations. In contrast, if the scheduled reserves are too few, load curtailment cannot be properly carried out under uncertainty realizations of relatively large values, which will result in higher operation costs. Therefore, the balancing point should be found to minimize the average operation cost with respect to the uncertainties. As shown in Fig. 8, the reserves scheduled by the proposed model in Case A-IV are fewer than those in Case A-III and more than those in Cases A-I and A-II. Because of the reduced load curtailment reserve in Case A-IV in comparison with Case A-III, less load curtailment can be performed; thus, more EVA charging demands need to be delayed in Case A-IV than in Case A-III when uncertainties in Case A-IV take the realization considered in Case A-III. For space-saving purposes, load curtailment reserves are not presented in some of the following parts of Section V when they do not reveal valuable information. As this paper focuses on the coordination of EVA charging and load curtailments, some variables including the AVR outputs, active and reactive power flows, and node voltage are not shown to save space.

To further illustrate the idea of delaying EVA charging, EVA charging demands and power in Case A-III are shown in Fig. 9. It can be seen that some EVA charging demands in Hours 20 and 21 are delayed to Hour 22, which can be interpreted as the corresponding EVA charging demands in Hour 20 being delayed for 2 hours and the corresponding EVA charging demands in Hour 21 being delayed for 1 hour. It should be noted that although **the average** EVA charging power in Case A-IV and all cases considered in the following parts of Section V can also be calculated, it does not reflect the number of hours that EVA charging demands are delayed for because it is not a deterministic value as in Cases A-I to A-III but rather a statistical value for a series of different scenarios. In some scenarios, such as the uncertainty realization considered in Case A-I, no EVA charging demand is delayed. In some other scenarios, such as the uncertainty realizations considered in Cases A-II and A-III, EVA charging demands

may be delayed in different patterns. As EVA charging power can be deduced from the delayed EVA charging demand, it is not presented in all other cases considered in Section V to save space.

B. Effects of coordinating EVA charging

In this part, the cost coefficients of load curtailment reserves of all loads in all hours, that is, $c_{\text{cur}}^{t,i}$, are set to 1¢/kWh, and the compensation coefficients of delayed charging of all EVAs in all hours, that is, $c_{\text{EVA}}^{t,i}$, are set to 3¢/kWh. Two cases as shown in Table III are considered in this part to study the effects of coordinating EVA charging. In Case B-I, no EVA charging demand is delayed, as shown in Fig. 10, because coordinating EVA charging is not allowed, and load curtailments are carried out according to Fig. 11 to ensure secure distribution system operation during peak hours. In contrast, EVA charging demands are delayed when EVA charging can be coordinated in Case B-II, and no load curtailment is carried out because of the relatively low compensation coefficient of delaying EVA charging. In some other settings, load curtailment and delayed EVA charging may be performed simultaneously, as shown in the following parts of Section V.

TABLE III CASES CONSIDERED IN SECTION V.B

Case	B-I	B-II
Coordinating EVA charging?	No	Yes

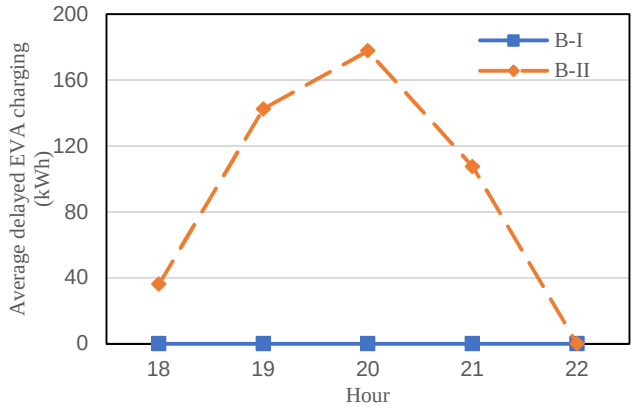

FIGURE 10. Average delayed EVA charging under different settings in Section V.B

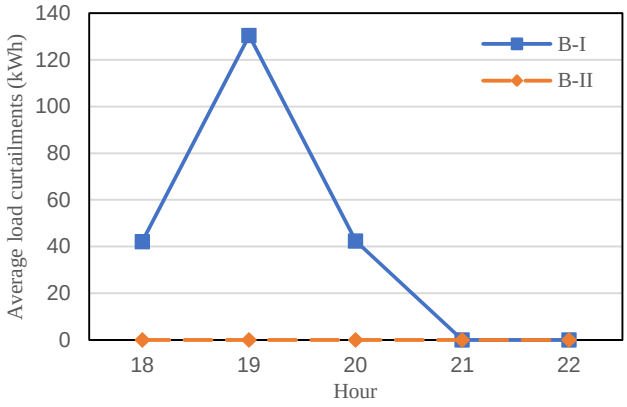

FIGURE 11. Average load curtailments under different settings in Section V.B

C. Varying compensation coefficients for delayed EVA charging

In this part, the cost coefficients of the load curtailment reserves of all loads in all hours, that is, $c_{\text{cur}}^{t,i}$, are set to 1¢/kWh, and the compensation coefficients of delayed EVA charging, that is, $c_{\text{EVA}}^{t,i}$, are set to varying values, as shown in Table IV. Relevant results are shown in Figs. 12 and 13. It can be seen that there is only delayed EVA charging but no load curtailment under Case C-I, which illustrates that delaying EVA charging is more economical than curtailing loads in this case. However, as delaying EVA charging becomes more expensive under Cases C-II to C-IV, the average delayed EVA charging decreases and average load curtailments increase to achieve the optimal overall costs.

TABLE IV CASES CONSIDERED IN SECTION V.C

Case	C-I	C-II	C-III	C-IV
Compensation coefficients for delayed charging of all EVAs in all hours, $c_{\mathrm{EVA}}^{t,i}$ (¢/kWh)	3	6	9	12

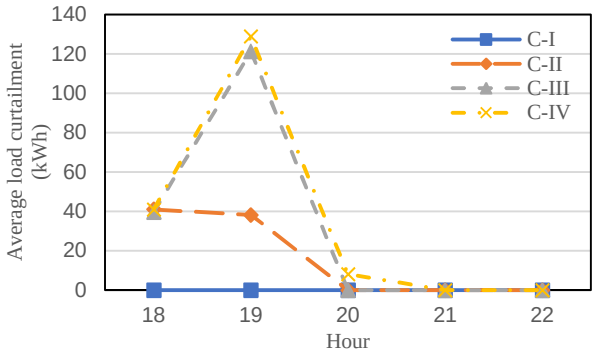

FIGURE 12. Average load curtailments under different settings in Section V.C

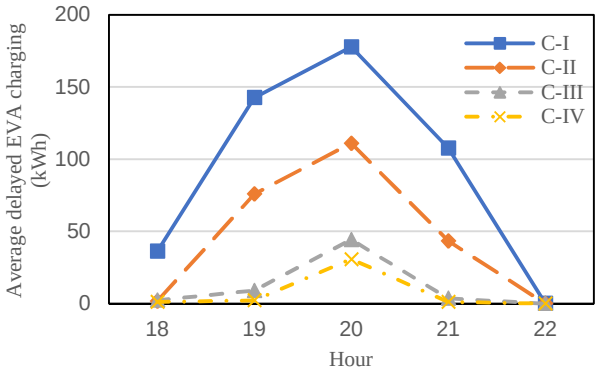

FIGURE 13. Average delayed EVA charging under different settings in Section V.C

D. Varying cost coefficients of load curtailment reserve

Another four cases are considered in this part as shown in Table V. Compensation coefficients of delayed charging of all EVAs in all hours, that is, $c_{\mathrm{EVA}}^{t,i}$, are set to 12¢/kWh. When the cost coefficients of load curtailment reserves, that is, $c_{\mathrm{cur}}^{t,i}$, decrease, curtailing loads becomes more economical and delaying EVA charging becomes relatively less economical, which results in less average delayed EVA charging, as shown in Fig. 14. At the same time, the load curtailment reserves increase to enable more load curtailments, as shown in Fig. 15. Compared with Cases D-I to D-III, the load curtailment reserves greatly increase in Case D-IV because delaying EVA charging is completely abandoned in Case D-IV. According to Fig. 16, the average load curtailments increase as the load curtailment reserves become cheaper, but the increase in the average load curtailments in Case D-IV is not as significant as that in load curtailment reserves. This is because load curtailment reserves need to be scheduled for the worst uncertainty realization, although it rarely occurs.

TABLE V CASES CONSIDERED IN SECTION V.D

Case	D-I	D-II	D -III	D -IV
Cost coefficients of load curtailment reserves of all loads in all hours, $c_{\mathrm{cur}}^{t,i}$ (¢/kWh)	1	0.75	0.5	0.25

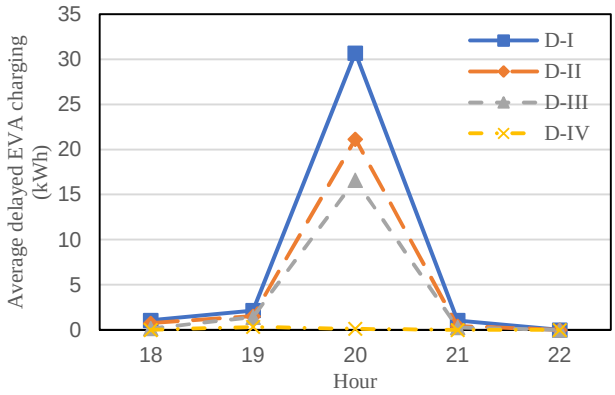

FIGURE 14. Average delayed EVA charging under different settings in Section V.D

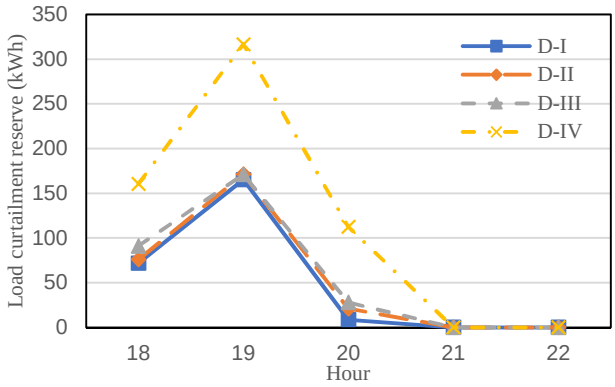

FIGURE 15. Load curtailment reserves under different settings in Section V.D

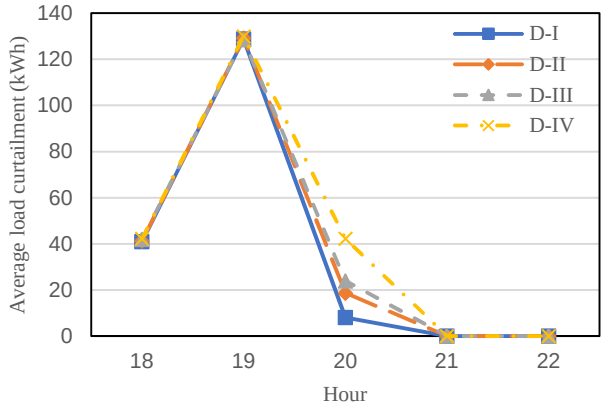

FIGURE 16. Average load curtailments under different settings in Section V.D

E. Varying limits on AVR output

Case studies are conducted in this part under varying limits on the AVR output, that is, l^{i}_{AVR}, as shown in Table VI. According to the solution algorithm presented in Section IV, the optimal first-stage decisions are obtained by iteratively generating optimality cuts and feasibility cuts. However, unlike optimality cuts, feasibility cuts may not be generated in some circumstances, such as Case E-I, as recorded in Table VII. This is because with sufficient reactive power output from AVRs under Case E-I, the proposed model is feasible in the second stage, even when no load curtailment reserve is scheduled in the first stage. In other words, there is no need to generate feasibility cuts to guarantee the feasibility of the second-stage problem. However, as the limits on the AVR output become tighter in Cases E-II to E-IV, the voltage drop on the distribution network could become quite significant, and thus the second-stage problem could be infeasible if load curtailments cannot be properly carried out. Because load curtailments in the second stage require corresponding load curtailment reserves to be scheduled in the first stage, feasibility cuts are generated when the proposed model is solved under Cases E-II to E-IV, as recorded in Table VII, to ensure that proper first-stage decisions can be made, and thus the second-stage problem will be feasible.

TABLE VI CASES CONSIDERED IN SECTION V.E

Case	E-I	E-II	E -III	E -IV
Limits on outputs of all AVRs, l^i_{AVR} (kVar)	500	400	300	200

TABLE VII WHETHER FEASIBILITY CUTS ARE GENERATED

Case	E-I	E-II	E -III	E -IV
Feasibility cuts generated?	No	Yes	Yes	Yes

According to Fig. 17, the hours with load curtailments expand and more loads are curtailed on average as limits on AVR output become tighter. But different from average load curtailments, average delayed EVA charging increases in the later hours while decreases in the earlier hours as limits on AVR output become tighter, as shown in Fig. 18. This is because, unlike load curtailments, delayed EVA charging needs to be recovered later, and thus causes correlations between different hours. More specifically, EVA charging demands in the earlier hours need to be delayed for a longer time, with greater corresponding costs, when the distribution network becomes more congested under tightened limits on AVR output, which makes delaying EVA charging in the earlier hours less economical. While in the later hours, EVA charging demands do not need to be delayed for a long time because the peak of overall loads in the distribution system has passed and loads start to decrease. Therefore, delaying EVA charging is economical in the later hours. To tackle the influences of tightened limits on AVR output, more EVA charging demands are delayed, on average, in the later hours. Therefore, instead of expanding as the curve in Fig. 17, the curve of the average delayed EVA charging in Fig. 18 moves to later hours as limits on AVR output become tighter. For similar reasons, the curves of the average delayed EVA charging also peak at different hours in some other cases considered in Section V. It should be noted that although load curtailment does not directly cause correlation between different hours, it interacts with and is thus influenced by delayed EVA charging. As a result, the curves of average load curtailments may peak at different hours as well. When the peaking hours of the delayed EVA charging curves are the same, load curtailments are still influenced by delayed EVA charging and thus may still have different peaking hours.

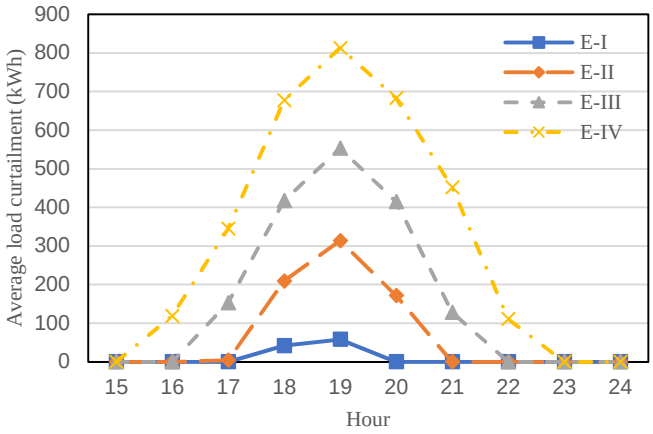

FIGURE 17. Average load curtailments under different settings in Section V.E

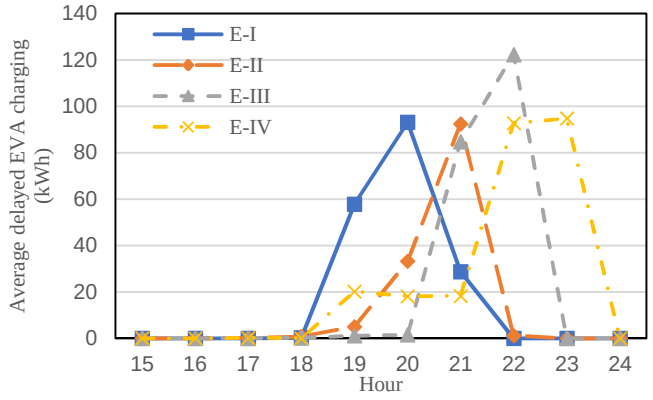

FIGURE 18. Average delayed EVA charging under different settings in Section V.E

F. Varying load level

Four cases are considered here by varying the loads $p_{\text{load}}^{t,i}$ as shown in Table VIII. According to Fig. 19 and 20, there is only delayed EVA charging but no load curtailments in Case F-I, which shows that delaying EVA charging is more economical than curtailing loads in this case. However, when the loads increase in Case F-II, there are both delayed EVA charging and load curtailments. It should be noted that no feasibility cut is added when the proposed model is solved under Cases F-I and F-II, which means that there is no need to curtail loads to guarantee the feasibility of the second-stage problem. Therefore, the load curtailments in Case F-II indicate that delaying EVA charging becomes less economical in Case F-II than in Case F-I. This is because some EVA charging demands need to be delayed for a longer time when the distribution network becomes more congested under increased loads in Case F-II. As the loads further increase in Case F-III, both the delayed EVA charging and load curtailments increase. However, when the distribution network becomes very congested under further increased loads in Case F-IV, delaying EVA charging becomes uneconomical in the earlier hours, which is the same as in Section V.E. Therefore, there is no delayed EVA charging but significant load curtailments during these hours.

TABLE VIII CASES CONSIDERED IN SECTION V.F

Case	F-I	F-II	F -III	F -IV
Loads at all nodes in all hours, $p_{\text{load}}^{t,i}$ (times of the original values)	0.9	1	1.1	1.2

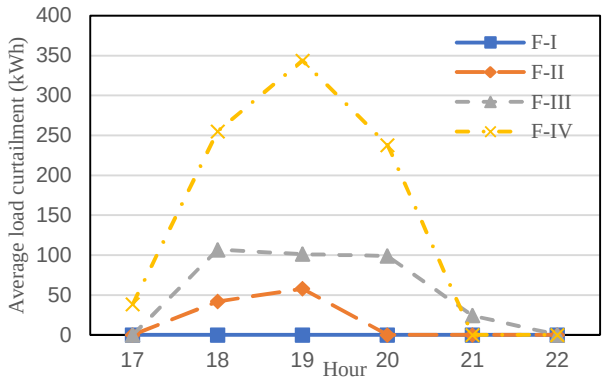

FIGURE 19. Average load curtailments under different settings in Section V.F

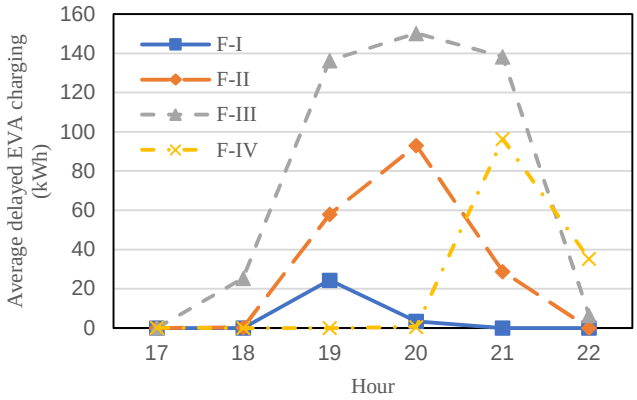

FIGURE 20. Average delayed EVA charging under different settings in Section V.F

G. Varying covariance matrix of uncertain EVA charging demands

In this part, case studies are based on a varying covariance matrix of uncertain EVA charging demands, that is, $\boldsymbol{\Sigma}$, as shown in Table IX. When the covariance matrix becomes larger, the fluctuation level of EVA charging demands increases, which means that the possibilities of both higher and lower EVA charging demands increase. To hedge against possible higher EVA charging demands, load curtailment reserves increase when the covariance matrix becomes larger, as shown in Fig. 21. With the increase in load

curtailment reserves, it becomes possible in Cases G-II to G-IV to reduce operation costs by curtailing more loads on average compared with Case G-I, as shown in Fig. 22. In other words, the task of guaranteeing system security under the worst possible uncertainty realization requires more load curtailment reserves to be scheduled for the more uncertain EVA charging demand, which thus covers the costs of load curtailment reserves for other uncertainty realizations in Cases G-II to G-IV. Therefore, curtailing loads becomes relatively more economical for most uncertainty realizations, and thus the average load curtailments increase in Cases G-II to G-IV compared with Case G-I. However, the average load curtailments in Cases G-II to G-IV are almost the same because EVA charging demands have the same average, although their covariance matrices vary in different cases. In addition, because of the increase in average load curtailments, the average delayed EVA charging decreases in Cases G-II to G-IV in comparison with Case G-I, as shown in Fig. 23.

TABLE IX CASES CONSIDERED IN SECTION V.G

Case	G-I	G-II	G -III	G -IV
Covariance matrix of uncertain EVA charging demands, $\boldsymbol{\Sigma}$ (times of the original values)	1	2	3	4

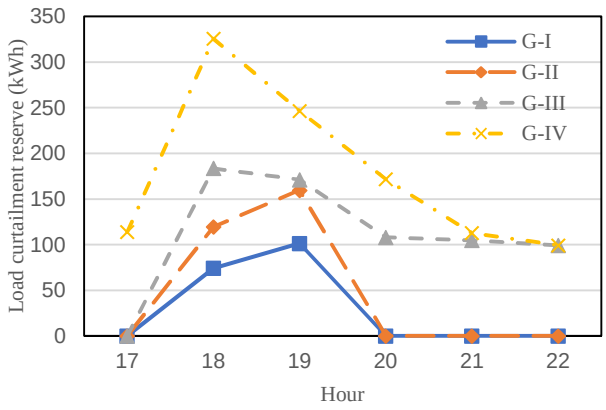

FIGURE 21. Load curtailment reserves under different settings in Section V.G

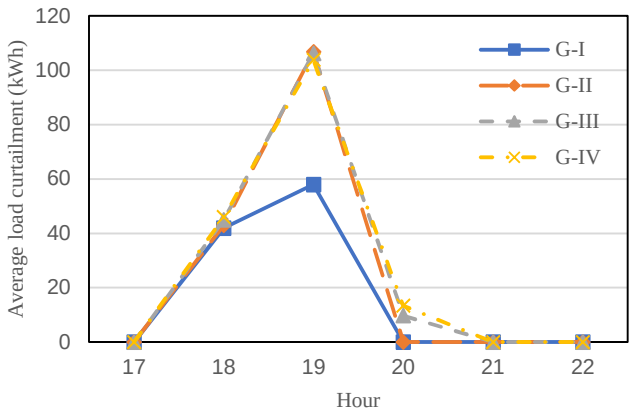

FIGURE 22. Average load curtailments under different settings in Section V.G

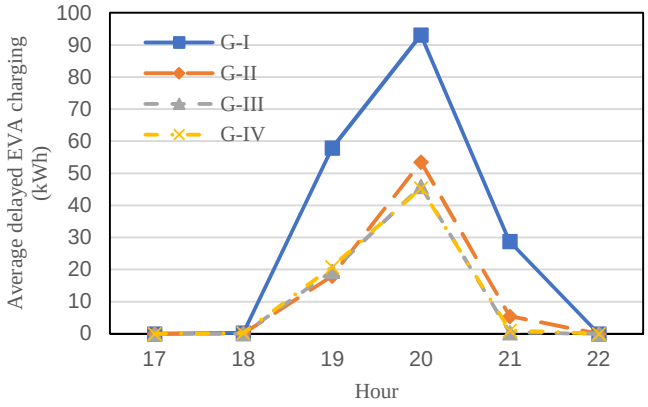

FIGURE 23. Average delayed EVA charging under different settings in Section V.G

H. Varying limits on delayed EVA charging

As shown in Table X, limits on delayed EVA charging, that is, $l_{\text{delay}}^{t,i}$, vary in the four cases considered in this part. The compensation coefficients of delayed charging of all EVAs in all hours, that is, $c_{\text{EVA}}^{t,i}$, are set to 2¢/kWh. Loads at all nodes in all hours, $p_{\text{load}}^{t,i}$, are set to 1.2 times the original values. As shown in Fig. 24, as the limits become tighter, more load curtailment reserves are prepared so that load curtailments can increase to compensate for the reduction in delayed EVA charging when the worst realization of uncertain EVA charging demands occurs. According to Fig. 25 and 26, the average load curtailments and average delayed EVA charging are barely influenced by the tightened limits on delayed EVA charging in Case H-II. However, as the limits further get tighter in Cases H-III and H-IV, the average delayed EVA charging decreases, and the average load curtailments increase.

TABLE X CASES CONSIDERED IN SECTION V.H

Case	H-I	H-II	H-III	H-IV
Limits on delayed charging demands of all EVAs in all hours, $l_{\text{delay}}^{t,i}$ (times of statistically expected EVA charging demands, $\mu_{t,i}$)	2	1.5	1	0.5

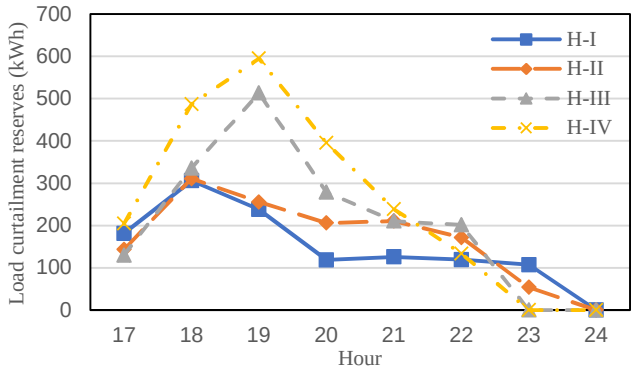

FIGURE 24. Load curtailment reserves under different settings in Section V.H

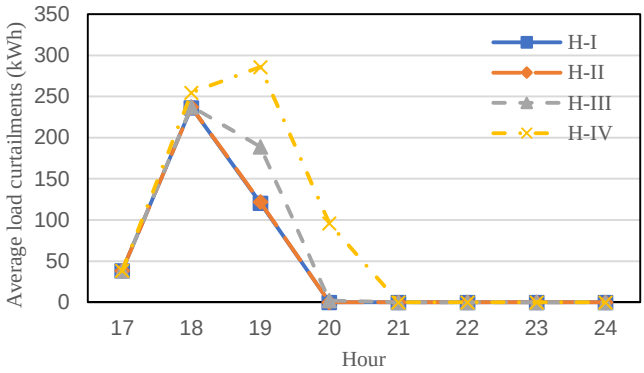

FIGURE 25. Average load curtailments under different settings in Section V.H

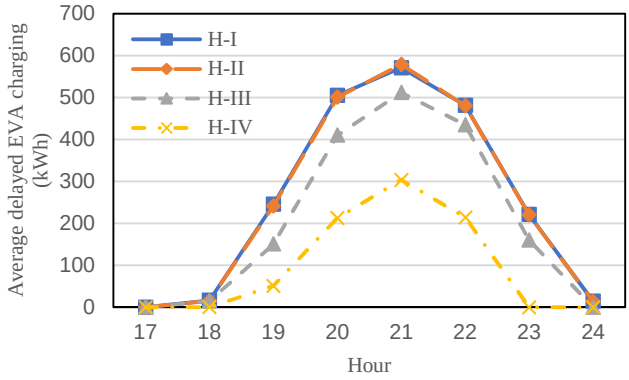

FIGURE 26. Average delayed EVA charging under different settings in Section V.H

VI. Conclusions

In this paper, a two-stage robust model is proposed to manage distribution system operation by coordinating EVA charging and load curtailments. With the cooperation of distributionally robust optimization and robust optimization, the proposed model optimizes the average economic performance and guarantees system security with respect to uncertain EVA charging demands. Depending on the parameter settings, either or both of delaying the EVA charging and curtailing loads are carried out to achieve the optimal result. Apart from the cost coefficients, the system load level also influences the relative advantages of delaying the EVA charging and curtailing loads over each other. As the load level increases, EVA charging demands need to be delayed for a longer time with greater corresponding costs, which makes delaying EVA charging less advantageous. In addition, when more load curtailment reserves are scheduled to guarantee system security, curtailing loads becomes relatively more economical, and thus average load curtailments may increase.

Appendix

Proof of Proposition 1:

Because S_ξ and U_1 are not empty, (39)-(41) is feasible. As discussed in Section III, (37) is equivalent to (32).

Let us assume that (39)-(41) is unbounded. Because S_ξ is an ellipsoid, $\boldsymbol{\xi}$ is bounded and thus $\boldsymbol{\xi}'\boldsymbol{H}^*\boldsymbol{\xi} + (\boldsymbol{h}^*)'\boldsymbol{\xi} + h_0$ in (39) is bounded from below. Because (39)-(41) is unbounded, $(\boldsymbol{b} - \boldsymbol{C}\cdot\boldsymbol{x}^* - \boldsymbol{D}\cdot\boldsymbol{\xi})'\boldsymbol{u}$ in (39) must be unbounded from above, which means that there must be a $\boldsymbol{u}_0 \in U_1$ and $\boldsymbol{\xi}_0 \in S_\xi$ such that $(\boldsymbol{b} - \boldsymbol{C}\cdot\boldsymbol{x}^* - \boldsymbol{D}\cdot\boldsymbol{\xi}_0)'\boldsymbol{u}_0 > 0$ and $\lambda\cdot\boldsymbol{u}_0 \in U_1$ for all $\lambda > 0$. According to the definition of U_1, as shown in (28), there must be $\boldsymbol{B}'\boldsymbol{u}_0 \le \boldsymbol{0}$. So, it can be known that $\boldsymbol{u}_0 \in U_2$, which contradicts (32). Therefore, (32) does not hold if (39)-(41) is unbounded. Equivalently, (39)-(41) is bounded if (32) holds.

Let us assume that (32) does not hold. Then, there is an $\boldsymbol{u}_0 \in U_2$ and $\boldsymbol{\xi}_0 \in S_\xi$ such that $(\boldsymbol{b} - \boldsymbol{C}\cdot\boldsymbol{x}^* - \boldsymbol{D}\cdot\boldsymbol{\xi}_0)'\boldsymbol{u}_0 > 0$. Obviously, as λ goes to plus infinity, $\lambda\cdot\boldsymbol{u}_0 \in U_1$ and $(\boldsymbol{b} - \boldsymbol{C}\cdot\boldsymbol{x}^* - \boldsymbol{D}\cdot\boldsymbol{\xi}_0)'\lambda\cdot\boldsymbol{u}_0$ is unbounded from above. As discussed in last

paragraph, $\boldsymbol{\xi}'\boldsymbol{H}^*\boldsymbol{\xi} + (\boldsymbol{h}^*)'\boldsymbol{\xi} + h_0$ in (39) is bounded from below. Therefore, (39)-(41) is unbounded if (32) does not hold. Equivalently, (32) holds if (39)-(41) is bounded.

■

Proof of Proposition 2:

Let us name the set $\{\boldsymbol{u}|(\boldsymbol{b} - \boldsymbol{C}\cdot\ \boldsymbol{x}^* - \boldsymbol{D}\cdot\boldsymbol{\xi})'\boldsymbol{u} \leq 1, \boldsymbol{u} \in U_2\}$ by U_3 and the hyperplane $\{\boldsymbol{u}|(\boldsymbol{b} - \boldsymbol{C}\cdot\ \boldsymbol{x}^* - \boldsymbol{D}\cdot\boldsymbol{\xi})'\boldsymbol{u} = 1\}$ by P. Obviously, U_3 is polyhedral. As (42)-(45) is a linear optimization problem over $\boldsymbol{u}$ when $\boldsymbol{\xi}$ is fixed, the optimal $\boldsymbol{u}$ obtained from (42)-(45) must be an extreme point of U_3.

As the only extreme point of U_2 is the origin point, all extreme points of U_3, except the origin point, must be at the intersection of P and U_2. Let us assume that $\boldsymbol{u}_0$ is at the intersection of P and U_2.

If $\boldsymbol{u}_0$ is in the interior of U_2, two points $\boldsymbol{u}_1$ and $\boldsymbol{u}_2$ can obviously be found at the intersection of P and U_2 such that $\boldsymbol{u}_0 = \lambda\boldsymbol{u}_1 + (1-\lambda)\boldsymbol{u}_2, 0 < \lambda < 1$; thus, $\boldsymbol{u}_0$ is not an extreme point of U_3. Therefore, the extreme points of U_3 cannot be in the interior of U_2 and must be on the faces of U_2.

If $\boldsymbol{u}_0$ is on a face of U_2, it will be at the intersection of P and this face of U_2. If the dimension of this face of U_2 is larger than 1, the dimension of the intersection of P and this face of U_2 will be larger or equal to 1. Therefore, two points $\boldsymbol{u}_1$ and $\boldsymbol{u}_2$ can be found at the intersection of P and this face of U_2 such that $\boldsymbol{u}_0 = \lambda\boldsymbol{u}_1 + (1-\lambda)\boldsymbol{u}_2, 0 < \lambda < 1$. Thus, $\boldsymbol{u}_0$ is not an extreme point of U_3 unless $\boldsymbol{u}_0$ is also on a 1-dimension face of U_2. Therefore, the extreme points of U_3 must be at the origin point or on a 1-dimension face of U_2, which is just an extreme ray of U_2 because U_2 is a polyhedral cone [45].

■

TABLE A PARAMETERS OF THE ADOPTED DISTRIBUTION NETWORK

Line No.	From Bus	To Bus	Resistance (Ω)	Reactance (Ω)
1	1	2	0.0922	0.0477
2	2	3	0.493	0.2511
3	3	4	0.366	0.1864
4	4	5	0.3811	0.1941
5	5	6	0.819	0.707
6	6	7	0.1872	0.6188
7	7	8	1.7114	1.2351
8	8	9	1.03	0.74
9	9	10	1.04	0.74
10	10	11	0.1966	0.065
11	11	12	0.3744	0.1238
12	12	13	1.468	1.155
13	13	14	0.5416	0.7129
14	14	15	0.591	0.526
15	15	16	0.7463	0.545
16	16	17	1.289	1.721
17	17	18	0.732	0.574
18	2	19	0.164	0.1565
19	19	20	1.5042	1.3554
20	20	21	0.4095	0.4784
21	21	22	0.7089	0.9373
22	3	23	0.4512	0.3083
23	23	24	0.898	0.7091
24	24	25	0.896	0.7011
25	6	26	0.203	0.1034
26	26	27	0.2842	0.1447
27	27	28	1.059	0.9337
28	28	29	0.8042	0.7006
29	29	30	0.5075	0.2585

30	30	31	0.9744	0.963
31	31	32	0.3105	0.3619
32	32	33	0.341	0.5302

Acknowledgements

This work was supported in part by the National Key Research and Development Project (2020YFE0200400), the National Natural Science Foundation of China (52077075), the Jiangsu Basic Research Project (BK20180284), and the Fundamental Research Funds for the Central Universities (2019MS007).

References

[1] J. P. Morgan, "Driving into 2025: The Future of Electric Vehicles." [Online]. Available: https://www.jpmorgan.com/global/research/electric-vehicles [accessed 29 September 2020]

[2] D. Raghunandan, "India Plans to Sell Only Electric Cars by 2030." [Online]. Available: https://www.newsclick.in/india-plans-sell-only-electric-cars-2030 [accessed 29 September 2020]

[3] N. Z. Xu and C. Y. Chung, "Uncertainties of EV Charging and Effects on Well-Being Analysis of Generating Systems," in IEEE Transactions on Power Systems, vol. 30, no. 5, pp. 2547-2557, Sept. 2015.

[4] Y. Nie, C. Y. Chung and N. Z. Xu, "System State Estimation Considering EV Penetration With Unknown Behavior Using Quasi-Newton Method," in IEEE Transactions on Power Systems, vol. 31, no. 6, pp. 4605-4615, Nov. 2016.

[5] K. Clement-Nyns, E. Haesen, and J. Driesen, “The impact of charging plug-in hybrid electric vehicles on a residential distribution grid,” IEEE Trans. Power Syst., vol. 25, no. 1, pp. 371–380, Feb. 2010.

[6] J. Hernández, F. Ruiz-Rodriguez, and F. Jurado, "Modelling and assessment of the combined technical impact of electric vehicles and photovoltaic generation in radial distribution systems," Energy, vol. 141, pp. 316-332, 2017.

[7] H. Fathabadi, "Utilization of electric vehicles and renewable energy sources used as distributed generators for improving characteristics of electric power distribution systems," Energy, vol. 90, pp. 1100-1110, 2015.

[8] S. Tabatabaee, S. S. Mortazavi, and T. Niknam, "Stochastic scheduling of local distribution systems considering high penetration of plug-in electric vehicles and renewable energy sources," Energy, vol. 121, pp. 480-490, 2017.

[9] C. Sabillón Antúnez, J. F. Franco, M. J. Rider and R. Romero, "A New Methodology for the Optimal Charging Coordination of Electric Vehicles Considering Vehicle-to-Grid Technology," in IEEE Transactions on Sustainable Energy, vol. 7, no. 2, pp. 596-607, April 2016.

[10] Y. Luo, G. Feng, S. Wan, S. Zhang, V. Li, and W. Kong, "Charging scheduling strategy for different electric vehicles with optimization for convenience of drivers, performance of transport system and distribution network," Energy, vol. 194, p. 116807, 2020.

[11] Q. Huang, Q. Jia, and X. Guan, “A multi-timescale and bilevel coordination approach for matching uncertain wind supply with EV charging demand,” in IEEE Trans. Autom. Sci. Eng., vol. 14, no. 2, pp. 694–704, Apr. 2017.

[12] X. Gao, K. W. Chan, S. Xia, B. Zhou, X. Lu, and D. Xu, "Risk-constrained offering strategy for a hybrid power plant consisting of wind power producer and electric vehicle aggregator," Energy, vol. 177, pp. 183-191, 2019.

[13] S. Z. Moghaddam and T. Akbari, "Network-constrained optimal bidding strategy of a plug-in electric vehicle aggregator: A stochastic/robust game theoretic approach," Energy, vol. 151, pp. 478-489, 2018.

[14] Z. Xu, W. Su, Z. Hu, Y. Song and H. Zhang, "A Hierarchical Framework for Coordinated Charging of Plug-In Electric Vehicles in China," in IEEE Transactions on Smart Grid, vol. 7, no. 1, pp. 428-438, Jan. 2016.

[15] W. Yao, J. Zhao, F. Wen, Y. Xue, and G. Ledwich, "A Hierarchical Decomposition Approach for Coordinated Dispatch of Plug-in Electric Vehicles," IEEE Transactions on Power Systems, vol. 28, no. 3, pp. 2768-2778, 2013.

[16] J. Zhao, J. Wang, Z. Xu, C. Wang, C. Wan, and C. Chen, “Distribution network electric vehicle hosting capacity maximization: a chargeable region optimization model,” IEEE Trans. Power Syst., vol. 32, no. 5, pp. 4119–4130, Sep. 2017.

[17] X. Lu, K. W. Chan, S. Xia, X. Zhang, G. Wang and F. Li, "A Model to Mitigate Forecast Uncertainties in Distribution Systems Using the Temporal Flexibility of EVAs," in IEEE Transactions on Power Systems, vol. 35, no. 3, pp. 2212-2221, May 2020.

[18] J. Zhang, X. Zhu, T. Chen, Y. Yu, and W. Xue, "Improved MOEA/D Approach to Many-objective Day-ahead Scheduling with Consideration of Adjustable Outputs of Renewable Units and Load Reduction in Active Distribution Networks," Energy, p. 118524, 2020.

[19] Y. Zhang, S. Shen, and J. L. Mathieu, “Distributionally robust chance constrained optimal power flow with uncertain renewables and uncertain reserves provided by loads,” IEEE Trans. Power Syst., vol. 32, no. 2, pp. 1378–1388, Mar. 2017.

[20] Z. Wang, Q. Bian, H. Xin, and D. Gan, “A distributionally robust coordinated reserve scheduling model considering CVaR-based wind power reserve requirements,” IEEE Trans. Sustain. Energy, vol. 7, no. 2, pp. 625–636, Apr. 2016.

[21] S. Balderrama, F. Lombardi, F. Riva, W. Canedo, E. Colombo, and S. Quoilin, "A two-stage linear programming optimization framework for isolated hybrid microgrids in a rural context: The case study of the “El Espino” community," Energy, vol. 188, p. 116073, 2019.

[22] F. Si, Y. Han, Q. Zhao, and J. Wang, "Cost-effective operation of the urban energy system with variable supply and demand via coordination of multi-energy flows," Energy, p. 117827, 2020.

[23] J. Zhu, S. Huang, Y. Liu, H. Lei, and B. Sang, "Optimal Energy Management for Grid-connected Microgrids via Expected-Scenario-Oriented Robust Optimization," Energy, p. 119224, 2020.

[24] M. Dadashi, S. Haghifam, K. Zare, M.-R. Haghifam, and M. Abapour, "Short-term scheduling of electricity retailers in the presence of Demand Response Aggregators: A two-stage stochastic Bi-Level programming approach," Energy, p. 117926, 2020.

[25] Y. Wang, L. Tang, Y. Yang, W. Sun, and H. Zhao, "A stochastic-robust coordinated optimization model for CCHP micro-grid considering multi-energy operation and power trading with electricity markets under uncertainties," Energy, p. 117273, 2020.

[26] Q. P. Zheng, J. Wang and A. L. Liu, "Stochastic Optimization for Unit Commitment—A Review," in IEEE Transactions on Power Systems, vol. 30, no. 4, pp. 1913-1924, July 2015.

[27] E. Delage and Y. Ye, "Distributionally robust optimization under moment uncertainty with application to data-driven problems," Operations research, vol. 58, no. 3, pp. 595-612, 2010.

[28] S. Zymler, D. Kuhn, and B. Rustem, "Distributionally robust joint chance constraints with second-order moment information," Mathematical Programming, vol. 137, no. 1-2, pp. 167-198, 2013.

[29] Y. Zhang, Y. Liu, S. Shu, F. Zheng, and Z. Huang, "A data-driven distributionally robust optimization model for multi-energy coupled system considering the temporal-spatial correlation and distribution uncertainty of renewable energy sources," Energy, p. 119171, 2020.

[30] Y. Zhang, Z. Huang, F. Zheng, R. Zhou, J. Le, and X. An, "Cooperative optimization scheduling of the electricity-gas coupled system considering wind power uncertainty via a decomposition-coordination framework," Energy, vol. 194, p. 116827, 2020.

[31] N. Rezaei, A. Khazali, M. Mazidi, and A. Ahmadi, "Economic energy and reserve management of renewable-based microgrids in the presence of electric vehicle aggregators: A robust optimization approach," Energy, p. 117629, 2020.

[32] X. Lu, Z. Liu, L. Ma, L. Wang, K. Zhou, and S. Yang, "A robust optimization approach for coordinated operation of multiple energy hubs," Energy, vol. 197, p. 117171, 2020.

[33] X. Zhu, B. Zeng, H. Dong, and J. Liu, "An interval-prediction based robust optimization approach for energy-hub operation scheduling considering flexible ramping products," Energy, vol. 194, p. 116821, 2020.

[34] J. Tan, Q. Wu, W. Wei, F. Liu, C. Li, and B. Zhou, "Decentralized robust energy and reserve Co-optimization for multiple integrated electricity and heating systems," Energy, p. 118040, 2020.

[35] S. Zhou et al., "Optimized operation method of small and medium-sized integrated energy system for P2G equipment under strong uncertainty," Energy, p. 117269, 2020.

[36] H. Zhang and P. Li, "Chance Constrained Programming for Optimal Power Flow Under Uncertainty," IEEE Transactions on Power Systems, vol. 26, no. 4, pp. 2417-2424, 2011.

[37] E. Delage and Y. Ye, "Distributionally robust optimization under moment uncertainty with application to data-driven problems," Operations research, vol. 58, no. 3, pp. 595-612, 2010.

[38] P. Zhao et al., “Volt-VAR-Pressure Optimization of Integrated Energy Systems with Hydrogen Injection,” in IEEE Transactions on Power Systems.

[39] P. Zhao, Y. Ding, C. Gu, H. Liu, Y. Bian and S. Li, "Cyber-Resilience Enhancement and Protection for Uneconomic Power Dispatch under Cyber-Attacks," in IEEE Transactions on Power Delivery.

[40] C. Zhang, Y. Xu, Z. Y. Dong and J. Ma, "Robust Operation of Microgrids via Two-Stage Coordinated Energy Storage and Direct Load Control," in IEEE Transactions on Power Systems, vol. 32, no. 4, pp. 2858-2868, July 2017.

[41] D. Bertsimas, X. V. Doan, K. Natarajan, and C.-P. Teo, "Models for minimax stochastic linear optimization problems with risk aversion," Mathematics of Operations Research, vol. 35, no. 3, pp. 580-602, 2010.

[42] A. Shapiro, "On duality theory of conic linear problems," in Semi-infinite programming: Springer, 2001, pp. 135-165.

[43] W. Wei, F. Liu, and S. Mei, "Distributionally Robust Co-Optimization of Energy and Reserve Dispatch," IEEE Transactions on Sustainable Energy, vol. 7, no. 1, pp. 289-300, 2016, doi: 10.1109/TSTE.2015.2494010.

[44] S. Boyd and L. Vandenberghe, Convex Optimization. Cambridge, U.K.: Cambridge Univ. Press, 2004.

[45] Ted Ralphs, "Advanced Operations Research Techniques IE316, Lecture 13"[Online]. Available: https://coral.ise.lehigh.edu/~ted/files/ie316/lectures/Lecture13.pdf [accessed 29 September 2020]

[46] Michael Patriksson, "Lecture 11: Benders Decomposition"[Online]. Available: http://www.math.chalmers.se/Math/Grundutb/CTH/tma521/0910/Lectures/fo11-beamer-2009.pdf [accessed 29 September 2020]

[47] Z. Caner Taskin, "Benders Decomposition"[Online]. Available: http://www.ie.boun.edu.tr/~taskin/pdf/taskin_benders.pdf [accessed 29 September 2020]

[48] J. Li, Z. Xu, J. Zhao, and C. Wan, “A coordinated dispatch model for distribution network considering PV ramp,” IEEE Trans. Power Syst., vol. 33, no. 1, pp. 1107–1109, 2018.

[49] A. Ben-Tal, L. El Ghaoui, and A. Nemirovski, Robust optimization. Princeton University Press, 2009.

[50] I. Polik and T. Terlaky, “A survey of the S-lemma,” ´ SIAM Rev., vol. 49, no. 3, pp. 371–418, 2007.

[51] J. Gorski, F. Pfeuffer, and K. Klamroth, “Biconvex sets and optimization with biconvex functions: A survey and extensions,” Math. Methods Oper. Res., vol. 66, no. 3, pp. 373–407, 2007.

[52] B. Venkatesh, R. Ranjan, and H. B. Gooi, “Optimal reconfiguration of radial distribution systems to maximize loadability,” IEEE Trans. Power Syst., vol. 19, no. 1, pp. 260–266, Feb. 2004.